# Comparison of Electron Transfer Dynamics in Molecule-to-Nanoparticle and Intramolecular Charge Transfer Complexes

**Yuhuang Wang,† Kun Hang, Neil A. Anderson, and Tianquan Lian***

*Department of Chemistry, Emory Univeristy, Atlanta, Georgia 30322*

*Received: April 8, 2003; In Final Form: June 17, 2003*

Ultrafast electron-transfer dynamics of a catechol−$TiO_2$ nanoparticle charge transfer (CT) complex and an intramolecular CT complex, $[Ti(cat)_3]^{2-}$ were compared. Both complexes show similar CT bands, suggesting similar donor (catechol) and acceptor(Ti) orbitals are involved in CT transition. However, the electron is localized on one Ti center in the $[Ti(cat)_3]$ complex, but can delocalize into other Ti centers in $TiO_2$ nanoparticles. The effect of charge delocalization on charge recombination dynamics was examined by comparing these complexes. In both cases, 400 nm excitation of the CT bands led to instantaneous promotion of an electron from a catechol ligand to a Ti(IV) center(s). In the molecular complex, the back electron-transfer dynamics from the Ti center to catechol ligand was observed on a 200 fs time scale. In the adsorbate-to-nanoparticle complex, back ET was much more complex, consisting of a 0.4 ps fast component and multiple slower components. The fast component was attributed to electrons trapped at or near the initial Ti centers, and slow components were attributed to trapped states farther away. Back ET kinetics from $TiO_2$ to a series of catechol derivatives were also compared. Although all kinetics were highly nonexponential, the average back ET rate became slower at larger driving force, consistent with ET in the Marcus inverted region.

## Introduction

Interfacial electron transfer (ET) between semiconductor nanoparticles and molecular adsorbate is a fundamental process relevant to many applications, such as solar energy conversion,[1,2] photocatalysis,[3] and nanoscale devices.[4] Many recent studies on dye-sensitized $TiO_2$ nanoparticles and thin films reveal that the electron injection from the excited state of strongly adsorbed dyes occurs on the ultrafast time scale. For example, in Ru(dcbpy)$_2$(NCS)$_2$-sensitized $TiO_2$ thin film, biphasic electron injection with a fast (<100 fs) and a slower picosecond component was observed.[5−11] Similar fast injection times have also been observed with dye-sensitized colloidal $TiO_2$ nanoparticles.[12−17] However, the reported back ET kinetics from $TiO_2$ to different dyes ranges from a few picoseconds[15−18] to milliseconds,[19−25] and from single[15−18] to multiexponential.[19,21,26−29]

There appear to be significant differences between back ET dynamics in nanocrystalline thin films and colloidal nanoparticles. In Ru polypyridyl dye-sensitized nanocrystalline $TiO_2$ thin films, back ET occurs on the microsecond to millisecond time scale.[19−25] Similarly, slow back ET was also observed in organic dye-sensitized $TiO_2$ nanocrystalline thin films.[20] Theoretical studies suggest that back ET in these materials is often controlled by the trapping/detrapping dynamics of the injected electrons.[30,31] Slow back ET results from infrequent encountering of the injected electron with the oxidized adsorbate. These dynamics are very different from those in colloidal $TiO_2$ nanoparticles, for which recombination processes on the picosecond time scale have been reported.[12−17,26,32] Back ET in the Fe(II)$(CN)_6^{4+}$-to-$TiO_2$ colloidal nanoparticle charge transfer complex was found to be highly nonexponential with time constants on the 1 ps, sub-nanosecond,[26,32] microsecond, and millisecond time scales.[27,33,34] The highly nonexponential kinetics, spanning 7 decades of time constants, have been attributed to a broad distribution of injected electrons at trap sites with varying energy and distance from the adsorbates.[26,32] The 1 ps back ET component is similar to that in many intramolecular CT complexes, such as $(NH_3)_5$Ru(III)−CNRu(II)$(CN)_5$ and related mixed valence dimers,[35−45] in which the electrons are localized in the metal center; while the slow components are comparable in time scale to those observed in nanocrystalline thin films, in which the electrons can diffuse in the interconnected network of nanoparticles.

The above comparison of back ET dynamics in intramolecular CT complexes, nanoparticle and nanocrystalline thin films may be suggestive of the notion that in nanocrystalline films, the ability of the injected electrons to separate farther away from the absorbate leads to slower charge recombination. Unfortunately, this comparison between nanocrystalline thin films and colloidal particles involves very different adsorbates, and the comparison with intramolecular CT complexes invokes unrelated ligands and metal centers. To further investigate the validity of the above notion, we are carrying out a series of studies that compares ET dynamics between the same adsorbate and nanomaterials of varying density of localized states. In a previous study we compared $TiO_2$ nanoparticles of different crystallinity.[12] Here, we report a comparison of ET dynamics of a catechol−$TiO_2$ nanoparticle CT complex with its molecular analogue, $[Ti(cat)_3]^{2-}$. The structure of the molecular complex resembles the surface binding sites of $TiO_2$−catechol complexes (Scheme 1). However, it has only one Ti(IV) center, serving as a model of a completely localized electron in a Ti atom. This is the first step in our plan to study ET in molecular model complexes with increasing numbers of titanium atoms.

* Author to whom correspondence should be addressed. E-mail: tlian@emory.edu.

† Current address: Department of Chemistry, Rice University, Houston, TX.

10.1021/jp034935o CCC: $25.00 
Published on Web 07/26/2003

**SCHEME 1: Schematic Structure of (a) Catechol−$TiO_2$ Complex and Its Derivatives, and (b) $[Ti(cat)_3]^{2-}$ Complex**

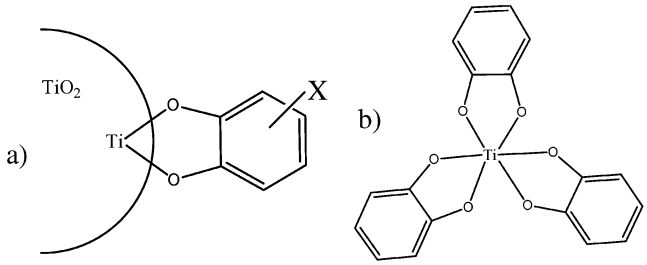


## Experimental Section

**Synthesis of a Model Complex.** $(NH_4)_2[Ti(cat)_3]$ was synthesized following a published procedure.[46] Catechol (Alfa, 99+%) and $TiCl_4$ (Aldrich, 99.9%) were used as received. The concentration of $(NH_4)_2[Ti(cat)_3]$ solution used for transient absorption measurements was 2 mM.

**Synthesis of $TiO_2$ Nanoparticles.** Nanometer-sized $TiO_2$ was prepared by following previously published synthetic methods.[26,47] Briefly, a 100 mL solution of titanium(IV) tetraisopropoxide (Aldrich, 97%) dissolved in isopropyl alcohol (5:95) was added dropwise (1 mL/min) under nitrogen to 900 mL of distilled water (0 °C) at pH 1.5 (adjusted with $HNO_3$). The solution was continuously stirred over several hours until a transparent colloid was formed. The colloidal solution was concentrated at 35−40 °C with a rotary evaporator and then dried with an air stream to yield a white powder. The sizes of the $TiO_2$ particles were measured by dynamic light scattering (Coulter Plus4) and were typically around 6 nm in diameter.

**Preparation of a Catechol−$TiO_2$ Colloidal Solution.** To form $TiO_2$/catechol complexes, $TiO_2$ nanoparticles and catechol (97%, Aldrich) were mixed with distilled and deaerated water to obtain a colloidal solution containing 20 g/L $TiO_2$ and 4 mM catechol. The solution was kept in the dark and protected by nitrogen. After stirring for 1 h, a deep red colored solution was formed and remained stable for a few days. A similar procedure was used for the series of five different catechol derivatives (shown in Scheme 1 and listed in Table 2). The stability of $TiO_2$/catechol and $(NH_4)[Ti(cat)_3]$ solution was monitored with UV−visible absorption. Negligible changes were observed within a couple of days.

**Laser System.** The femtosecond pump−probe spectrometer used for this study has been described in detail elsewhere.[26] Briefly, an 800 nm output pulse from the regeneratively amplified femtosecond Ti:sapphire laser (Clark-MXR, 1 kHz repetition rate at 800 nm, 100 fs) was split into two parts to generate pump and probe pulses. One part with 300 $\mu$J/pulse was frequency doubled in a BBO crystal to generate a pump beam at 400 nm. About 6 $\mu$J/pulse of the other part is focused onto a 2-mm thick sapphire window to generate a white light continuum. Slices of the white light with approximately 10 nm spectral width were selected by a variable interference filter (Optical Coating Laboratory Inc.) to provide a tunable probe pulse. Typically, the noise level of the white light was about 0.4% and the noise in the measured absorbance change was about 0.1−0.2%. The relative polarization of the pump and probe beams were set at the magic angle (54.7°) to ensure that the measured absorbance change was due to population dynamics only. The diameters of the pump and probe beams were about 500 $\mu$m and 220 $\mu$m, respectively. The samples were flowed through flow cells of 250 $\mu$m path length to avoid buildup of long-term photoproduct. The instrument response function of the experiment is well represented by a Gaussian function with 150 fs full width at half-maximum.

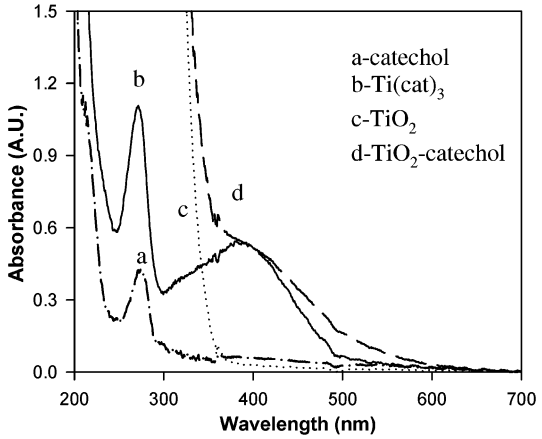


**Figure 1.** UV/Visible spectra for (a) catechol (dot−dash line), (b) $(NH_4)_2[Ti(cat)_3]$ (solid line), (c) bared $TiO_2$ (dotted line), and (d) $TiO_2$/catechol (dashed line) in water.

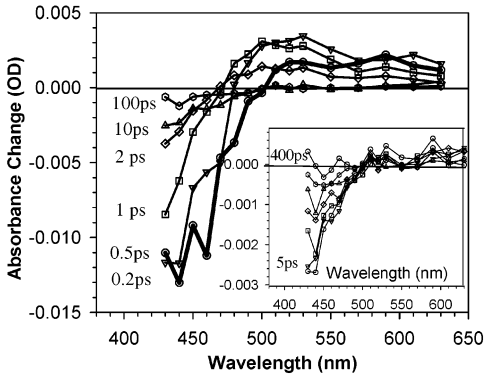


**Figure 2.** Transient difference absorption spectra of $[Ti(cat)_3]^{2-}$ in water at different delay times after 400 nm excitation. The inset shows the spectra between 5 and 400 ps.

## Results

Figure 1 shows the UV/visible spectra of a catechol/$TiO_2$ complex (dashed line) and $[Ti(cat)_3]^{2-}$ (solid line) in aqueous solution. For comparison, the spectra of $TiO_2$ colloid (dotted line) and catechol (dash−dot line) are also shown. The spectrum of $[Ti(cat)_3]^{2-}$ exhibits an ligand-to-metal charge transfer (LMCT) band centered at 388 nm and another band at 270 nm. The latter is also observed in the absorption spectrum of free catechol molecules. The position and extinction coefficient ($\epsilon$ = 9290 $mol^{-1}$ $cm^{-1}$) of the LMCT band agree well with previously reported values.[46] The catechol/$TiO_2$ complex shows, in addition to the absorption of $TiO_2$ at <360 nm, a broad new band centered at ~390 nm and extending farther into the visible range with an onset at ~600 nm. This band is attributed to the catechol-to-$TiO_2$ charge-transfer complex.[48−50]

Shown in Figure 2 are the transient absorption difference spectra of $[Ti(cat)_3]^{2-}$ in water at 0.2, 0.5, 1, 2, 10, and 100 ps after 400 nm excitation. At <5 ps, the difference spectra consist of a bleach at <460 nm and a broad absorption at 500−630 nm. At 200 fs, the broad absorption band is already formed, although it is featureless and extends beyond 630 nm. At delay times between 0.2 and 2 ps, it becomes narrower and shifts to shorter wavelength. This leads to an absorption decay at >550 nm, a bleach recovery at <460 nm, and a complex amplitude change from 460 to 550 nm. The inset of Figure 2 shows transient spectra between 5 and 400 ps. On this time scale, the

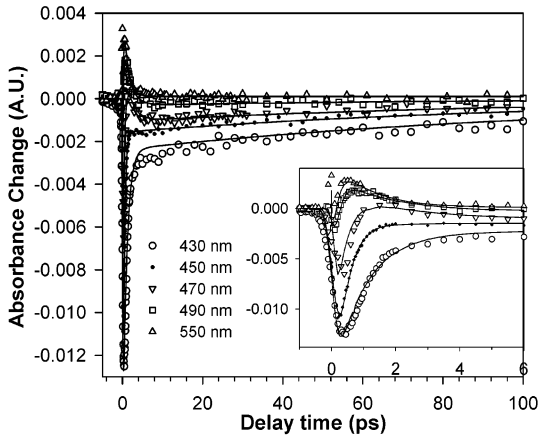


**Figure 3.** Transient kinetics of $[Ti(cat)_3]^{2-}$ measured at various wavelengths after 400 nm excitation. Open symbols are data, and solid lines are multiexponential fits to the data. Fitting parameters are listed in Table 1. The inset shows the same data on a shorter time scale.

**TABLE 1: Multiexponential Fitting Parameters for Bleach Recovery Kinetics of $[Ti(cat)_3]^{2-}$ at Various Probe Wavelengths**[a]

| wavelength | $\tau_1$ ($A_1$) | $\tau_2$ ($A_2$) | $\tau_3$ ($A_3$) |
|---|---|---|---|
| 430 | 1.0 (11.3) | | 80 (2.25) |
| 440 | 0.70 (15.0) | | 140 (2.0) |
| 450 | 0.40 (13.5) | | 100 (1.5) |
| 470 | 0.38 (12.2) | 1.80 (−3.2) | 100 (1.0) |
| 480 | 0.30 (12.5) | 1.50 (−5.2) | 100 (0.7) |
| 490 | 0.30 (9.0) | 1.45 (−4.5) | 100 (0.3) |
| 550 | 0.18 (9.5) | 1.10 (−4.7) | |

[a] Time constants are in ps and amplitudes are in mOD. The initial bleach occurs within instrument response time of 150 fs.

absorption at >500 nm becomes negligible. There remains only a small bleach at <500 nm that resembles the static UV/visible absorption spectrum of $[Ti(cat)_3]^{2-}$.

The dynamics of spectral blue shift and bleach recovery at early time were more carefully examined by measuring transient kinetics in the 430−550 nm region, as shown in Figure 3. After 5 ps, the kinetics traces are the same for all wavelengths consisting of a bleach recovery with ∼100 ps time constant. At <5 ps, the kinetics traces vary with the probe wavelengths. In the red side of the spectra (>500 nm), they show a fast rise of absorption signal that is followed by a fast decay. In the blue side (<450 nm), an instantaneous bleach and subsequent recovery was observed. In the overlap region (450−500 nm), an instantaneous bleach is followed by fast rise (recovery) and decay. The fitting parameters for these kinetics are listed in Table 1. The time constants for fast rise and decay become longer at shorter wavelengths, increasing from 0.18 and 1.1 ps at 550 nm to 0.38 ps and 1.8 ps at 470 nm. At 430 nm, only a 1.0 ps rise (bleach recovery) is observed at early time. These kinetics traces are consistent with the spectral evolution shown in Figure 2, i.e., at early time a nascent absorption band undergoes a continuous spectral blue-shift and narrowing that leads to bleach recovery. Because of this spectral blue shift and narrowing, the apparent rise time of absorption species becomes longer at shorter wavelengths. Therefore, the rise time at the longest wavelength (0.18 ps at 550 nm) represents the upper limit of formation time of the absorption band. For the same reason, the apparent bleach recovery time becomes longer at shorter wavelengths. The 1.0 ps recovery time at 430 nm, the shortest wavelength measured, represents the lower limit of the bleach recovery time.

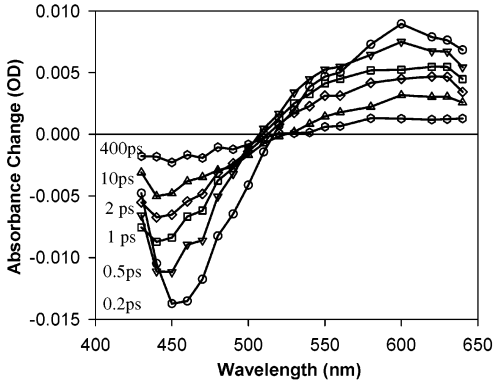


**Figure 4.** Transient difference absorption spectra of catechol/$TiO_2$ complex in water at 0.2, 0.5, 1, 2, 10, and 400 ps after 400 nm excitation. The spectrum at each delay time consists of a bleach signal and a positive absorption, separated by an isosbestic point at 504 nm. These features are attributed to the depletion of the CT transition and the absorption of injected electrons in $TiO_2$, respectively.

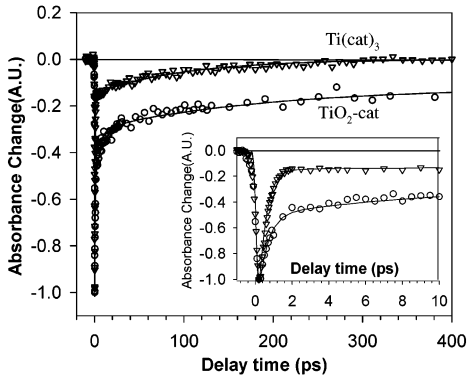


**Figure 5.** Bleach recovery kinetics measured at 450 nm after 400 nm excitation for catechol−$TiO_2$ (circles) and $(NH_4)_2[Ti(cat)_3]$ (triangles). The solid lines are multiexponential fits to the data. Fitting parameters are shown in Tables 1 and 2. Displayed in the inset are the same kinetics plotted on a shorter time scale.

Similar measurements were carried out for $TiO_2$−catechol complexes. Figure 4 shows the transient difference absorption spectra at 0.2, 0.5, 1, 2, 10, and 400 ps after 400 nm excitation. The spectrum at each delay time consists of a bleach at 430−510 nm and a transient absorption at 510−640 nm region, separated by a well-defined isosbestic point at around 504 nm. Except for the 0.2 ps trace, there is no significant spectral shift after 0.5 ps. The normalized difference spectra monitored at different delay times are the same within the signal-to-noise level.

Similarly, the normalized kinetics measured at different wavelengths agree with each other. Therefore, only kinetics at 450 nm are shown from now on. Shown in Figure 5 is the transient kinetics of $TiO_2$/catechol measured at 450 nm. The kinetics trace for $[Ti(cat)_3]^{2-}$ at the same wavelength is also shown for comparison. These traces have been scaled to have the same initial bleach magnitude. Displayed in the inset are the same normalized traces on a shorter time scale. The solid lines are the best multiexponential fits to the data. For $Ti(cat)_3^{2-}$, the data are well fit by a biexponential function with time constants (and amplitudes) of 0.40 ± 0.05 ps (90%) and 100 ± 20 ps (10%) as shown in Table 1. For $TiO_2$/catechol, at least four components are required: 0.40 ± 0.05 ps (62%), 8 ± 1 ps (19%), 200 ± 20 (11%), and ≫1 ns (8%). The kinetics after 1 ps can also be well fit by a stretch exponential function (William-Watts relation[51]) of the form $\exp[-(t/\tau_\beta)^\beta]$. The data

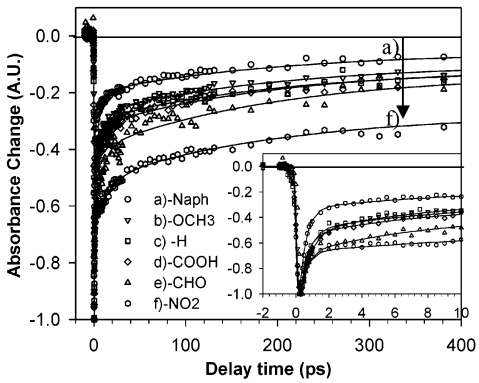


**Figure 6.** Comparison of normalized bleach-recovery kinetics (at 450 nm) for complexes formed between $TiO_2$ nanoparticles and (a) 2,3-dihydroxynaphathelene (circles), (b) 3-methoxycatechol (inverse triangles), (c) catechol (squares), (d) 3,4-dihydroxybenzoic acid (diamonds), (e) 3,4-dihydroxybenzaldehyde (triangles) and (f) 4-nitrocatechol (circles). The solid lines are multiexponential fits to the kinetics. The fitting parameters are listed in Table 2. Shown in the inset are the same kinetics traces on a shorter time scale.

**TABLE 2: Multiexponential Fitting Parameters and Average Back Electron Transfer Time Constants for CT Complexes between $TiO_2$ and Catechol Derivatives (catechol−X)[a]**

| | X | $E_{ox}$[b] (v, vs NHE) | $\Delta G$ (v) | fitting parameters 0.4 ps (%) | 8 ps (%) | 200 ps (%) | >1 ns (%) | average time[c] $\langle\tau\rangle$ (ps) |
|---|---|---|---|---|---|---|---|---|
| a | −naph[d] | 1.11 | −1.39 | 79.1 | 8.8 | 8.8 | 3.3 | 53.3 |
| b | 3-$OCH_3$ | 1.12 | −1.40 | 62.7 | 19.2 | 11.2 | 6.9 | 100.0 |
| c | −H | 1.18 | −1.46 | 62.2 | 18.9 | 10.8 | 8.1 | 113.5 |
| d | 4-COOH | 1.21 | −1.49 | 62.9 | 15.7 | 13.9 | 7.5 | 112.7 |
| e | 4-CHO | 1.25 | −1.53 | 51.5 | 20.5 | 18.7 | 9.3 | 145.7 |
| f | 4-$NO_2$ | 1.27 | −1.55 | 44.8 | 14.0 | 19.6 | 21.6 | 327.4 |

[a] Also shown are the standard one-electron oxidation potentials and back ET driving forces calculated from conduction band edge. [b] Estimated from standard two-electron redox potential from refs 52,53. [c] See main text. [d] 2,3-Dihydroxynaphthalene.

before 1 ps cannot be well described by the same stretched exponential function.

Negligible signals were observed in a $TiO_2/H_2O$ colloid or catechol solution under the same experimental condition, as expected from the lack of absorption at 400 nm in these samples (Figure 1). Pump-power dependence was also investigated. The signal size scaled linearly with excitation power over a range of factor of 3, indicating a one-photon excitation event. Furthermore, kinetics after normalizing for pump power were identical.

Back ET dynamics for $TiO_2$ nanoparticles sensitized by five catechol derivatives were also measured. Shown in Figure 6 is a comparison of ground-state bleach recovery kinetics measured at 450 nm. In all these systems, we observed highly non-single-exponential recovery kinetics. The simplest multiexponential fit requires four components with time constants of about 0.4 ps, 8 ps, 200 ps, and >1 ns. To facilitate comparison of nonexponential ET kinetics measured in different catechol derivatives, we fixed the time constants and let the preexponential factors vary in the fitting process. The fitting parameters are listed in Table 2.

## Discussion

**1. $[Ti(cat)_3]^{2-}$.** Optical excitation of the CT transition transfers electron density instantaneously from a catechol ligand to the Ti(IV) center, generating a catechol radical (benzosemiquinone, SQ) and a Ti(III). The charge-separated excited state will decay to regenerate the ground state through charge recombination (or back electron transfer). As shown in Figure 2, the transient difference spectra of $[Ti(cat)_3]^{2-}$ consists of a bleach of the ground-state CT band from 430 to 500 nm, and a transient absorption band in 500−630 nm. The latter blue shifts and narrows on a ~1 ps time scale. The absorption feature can result from the charge-separated excited state, $[Ti^{(III)}(cat)_2(SQ)]^{2-}$, or the hot ground-state molecule generated after charge recombination. In the charge-separated excited state, $[Ti^{(III)}(cat)_2(SQ)]^{2-}$, benzosemiquinone is not expected to absorb in this spectral region since the free form showed no absorption at wavelength longer than 380 nm.[54] It is unclear whether the CT transition of the charge-separated state falls in this region.

The transient absorption feature is consistent with a hot ground-state species, which has a red-shifted spectrum and undergoes continuous blue shift and narrowing toward the vibrationally relaxed ground-state position (bleach). The bleach recovery time (~1 ps) therefore reflects the vibrational cooling time on the ground electronic state. The formation time of the hot ground-state species represents the back ET time from the Ti(III) center to the catechol radical. The upper limit of the back ET time is given by the 180 ± 50 fs rise time at 550 nm, the longest wavelength measured. The kinetics at shorter wavelengths are slower because they also reflects the vibrational cooling process. Related effects of vibrational cooling on the transient absorption spectrum have been previously observed and carefully analyzed for molecules in solution.[55]

Ultrafast back ET has been observed in other charge-transfer complexes.[35−45] Previous studies of mixed valence transition metal dimers of Ru and Fe showed that back ET could occur on the 20 fs time scale.[38] Fast back ET is in agreement with strong electronic coupling between donor and acceptor states in these CT complexes. As dictated by the Franck−Condon overlap and driving force, ultrafast back ET is expected to generate vibrationally hot ground-state species and it has been observed in many CT complexes.[35,38,41] The reported picosecond relaxation times are typical of large molecules in similar solvent environments.[56,57]

Although over 80% of the bleach recovers within 2 ps, there remains a small component at later time. The transient spectra after 5 ps, shown in the inset of Figure 2, show a bleach peak in the 430−500 nm region with no apparent sign of other absorption species in the spectral window probed. The complete recovery of the bleach is well fit by an exponential function with 100 ps time constant, as shown in Figures 3 and 5. The origin of the slow bleach component is not clear. Similar slow dynamics were not reported in previous studies of mixed-valence transition metal complexes.[38,41] We speculate that in this system back ET is also completed within 1 ps, similar to other CT complexes,[38,41] but the excess vibrational energy may dissociate one of the Ti−O bonds in some of the complexes, reducing the strength of the CT transition and creating a bleach. The slow bleach recovery component then corresponds to reformation of the complexes. This type of ligand detachment and reattachment dynamics has been observed in a complex containing Rh−N bonds.[58]

**2. $TiO_2$/Catechol.** In the catechol−$TiO_2$ nanoparticle charge-transfer complexes, 400 nm excitation leads to the depletion of the ground-state CT complex, formation of electrons in $TiO_2$, and catechol radicals. Depletion of the ground state of the CT complex is clearly shown by the bleach signal at 420−510 nm, shown in Figure 4. The transient absorption signal at 510−650 nm is attributed to injected electrons in $TiO_2$. This assignment

is based on reported absorption features of injected electrons[47,59−63] and the lack of absorption of catechol radical cation in this region.[54] The absorption for electrons in $TiO_2$ has been observed by direct excitation of band gap transition[47,59−64] or by injection through electrochemical methods.[65,66] Previous studies also showed that electrons in collidal $TiO_2$ nanoparticles were trapped on the 200 fs time scale,[64] giving rise to a broad absorption in the 500−650 nm region in the picosecond time scale.[47,62,63] The nature of the trapped sites has also been investigated by EPR spectroscopy.[67] Signals for electrons both localized on and loosely bound to Ti(III) centers have been reported.

The bleach recovery and the absorption decay kinetics measured at different wavelengths from 420 to 640 nm are the same within the signal-to-noise of the data, indicating that the spectral evolution is dominated by the reformation of the ground-state CT complex (bleach recovery) and the corresponding disappearance of the injected electrons (absorption decay). There may be evidence for spectral blue shifting of the absorption feature in the <0.5 ps time scale, but it is not as pronounced as in $[Ti(cat)_3]^{2-}$. Back ET may also form hot ground-state complexes, but its spectral feature is not as noticeable because of overlap with the stronger absorption signal of electrons.

The back ET kinetics are highly nonexponential. Approximately 60% of the bleach recovers with a 0.4 ps time constant and the rest with a time constant from a few picoseconds to over 1 ns. Furthermore, the recombination kinetics on the <1 ns time scale are independent of the pump power, indicating that it is dominated by geminate pairs. Similar nonexponential recombination and pump power independent kinetics were observed in our previous study of $Fe((II)(CN)_6^{4-}/TiO_2$, in which excitation power was varied over a factor of 15.[32] This suggests that the back ET on the <1 ns time scale involves electrons located close to their parent adsorbates from which they were injected. The nonexponential behavior is attributed to a distribution of trap electrons, which gives rise to a distribution of back ET times. A more detailed discussion of the back ET dynamics is presented in the next section.

**3. Comparison of Back ET Dynamics in $TiO_2$−Catechol and $[NH_4]_2[Ti(cat)_3]$.** As shown in Figure 1, CT bands of the catechol-to-Ti molecular complex and catechol-to-$TiO_2$ nanoparticle complex are similar. In $[Ti(cat)_3]^{2-}$, the donor and acceptor orbitals are formally the catechol HOMO $\pi$ orbital and the empty 3d orbitals of Ti(IV) center, respectively. In the catechol−nanoparticle complex, the donor orbital is still the catechol HOMO $\pi$ orbital, but the nature of the accepting Ti orbitals in $TiO_2$ is less clear. The similarity of the CT bands may suggest that the acceptor orbitals in the nanoparticle are also localized on one or a few Ti(IV) centers. This notion is supported by quantum chemical calculation of adsorbates on $TiO_2$.[69,70] The acceptor state of the catechol−$TiO_2$(cluster) charge-transfer complex is dominated by Ti atoms near the adsorbate according to a recent INDO/S-CI calculation.[69] A DFT calculation of isonicotinic acid on a $TiO_2$ slab found that ∼20% of the acceptor state density was localized on a single Ti atom of the first surface layer.[70]

The energetics of the acceptor state can be estimated from the position of the CT band. The transition frequency for optically-induced ET in donor−acceptor CT complexes is related to the driving force and the reorganization energy of the ET process:[71]

$$h\nu_{op} = \lambda + \Delta G_0 = \lambda + [E_{ox}(\text{cat/cat}^+) - E(\text{Ti(IV)/Ti(III)})]$$

The transition frequency $h\nu_{op} = 3.2$ eV is determined from the peak of the CT band. Using the redox potential of a free catechol/benzosemiquinone pair of +1.1 V vs NHE[72] and assuming a reorganization $\lambda$ energy of 0.3−1 V, we estimate that the Ti(IV)/Ti(III) pair is located at −1.8 to −1.1 V vs NHE. This rough estimate locates the acceptor state significantly above the conduction band edge of $TiO_2$, which is −0.28 V (vs NHE) at pH = 2.[73]

While the acceptor states in the catechol−$TiO_2$ surface complex may involve only one or a few Ti sites, the empty Ti(IV) 3d orbitals interacts with each other to form a continuum of delocalized conduction band states.[74] This is in contrast to the localized acceptor state at the Ti(IV) center in $[Ti(cat)_3]^{2-}$. The effect of charge delocalization on back ET dynamics is demonstrated in Figure 5, in which the back ET kinetics of $[Ti(cat)_3]^{2-}$ and catechol−$TiO_2$ are compared. In the molecular complex, back ET occurs within 200 fs, followed by cooling of hot ground-state complexes, giving rise to a 0.4 ps bleach recovery time at 450 nm. In the catechol−$TiO_2$ CT complex, non-single-exponential and much slower recombination kinetics are observed. In addition to the 0.4 ps component, over 40% of the bleach recovers on a slower time scale. In this case, optical excitation also promotes an electron to one or a few Ti(IV) centers near the adsorbate. Back ET from these centers would be fast, similar to that in the molecular complex. We attribute the 0.4 ps recombination component to this process. However, the injected electrons can also rapidly delocalize to other Ti centers farther away from the adsorbate. They can be trapped at sites with a distribution of trap energy and distance from the absorbate, resulting in the observed nonexponential and slower recombination dynamics. Evidence of injected electrons at different distances from the adsorbate was provided in a recent EPR study.[68] A similar model of an initially localized injected electron wavepacket and subsequent delocalization to band states was previously proposed.[75]

The slow recombination components in $TiO_2$/catechol can also be fit by a stretch exponential function. Stretched exponential functions have often been used to model highly nonexponential kinetics.[76,77] The "stretching" parameter $\beta$ describes the width of the distribution of time constants. A $\beta$ value of 0.17 is obtained for our data, indicating a broad distribution of relaxation time. We attribute this to wide distribution of trap states on $TiO_2$. The effects of trap distribution on recombination kinetics have been examined in previous studies of recombination dynamics in $TiO_2$.[30,32,78] In a recent study, we demonstrated that back ET kinetics from $TiO_2$ to catechol could be affected by the distribution of trap states.[12] A smaller fast (0.4 ps) component and less recombination yield at 1 ns were observed in highly crystalline $TiO_2$ nanocrystals compared to less crystalline nanoparticles. We suggest that the smaller trap state density in the more crystalline materials may reduce the probability of an electron being trapped at the initial Ti(IV) sites and increase the probability of trapping at sites farther away from the adsorbates. This reduces the probability of recombination from the initial Ti centers (the 0.4 ps component) and decreases the rate of the slower recombination components. This trend is consistent with the difference between catechol−$TiO_2$ and its molecular analogue. These results point to the important effect of charge delocalization on recombination dynamics in nanoparticles.

**4. Marcus Inverted Region.** As shown in Figure 6 and Table 2, back ET from $TiO_2$ to a series of catechol derivatives appears to be slower for adsorbates with more positive redox potentials. The trend suggests a dependence of back ET on driving force. Since back ET probably involves a distribution of trap states, there should be a distribution of driving forces. We previously

estimated that, within 1 ns, injected electrons could relax to trap states with energies as much as 0.3 eV below the conduction band edge.[32] To facilitate comparison, we calculate the driving force for back ET for electrons at the conduction band edge:

$$\Delta G_0 = -[E_o(\text{adsorbate}) - E_{CB}(TiO_2)]$$

$E_o$ is the one-electron oxidation potential of catechol and derivatives. Its value has not been well determined, but it was estimated [to] be about 0.38 V lower than the standard two-electron redox potential $E_o$.[52,53] Using an $E_{CB}$ value of $-0.28$ V (vs NHE) for $TiO_2$ nanoparticles at pH = 2,[73] and the estimated standard one-electron oxidation potential of catechol derivatives, we can calculate the driving force for the back ET reaction from the conduction band edge. As shown in Table 2, for the series studied, the redox potential changes from $+1.11$ to $+1.27$ V (vs NHE), corresponding to a change in back ET driving force from ca. $-1.39$ to $-1.55$ eV. We thus expect that the back ET process will fall in the Marcus inverted regime. It should be noted, for the reason discussed above, that the estimated driving forces for back ET may be higher than the actual values, but they should qualitatively reflect the trend for this series of catechol derivatives.

As can be seen from Figure 6 and Table 2, as the driving force for back ET increases, the back ET kinetics becomes slower. This is reflected by the decreasing percentage of bleach recovery within 1 ns, which indicates an increase of relative amplitude of the slow (>1 ns) components. We have attempted a more quantitative comparison of the back ET rates by calculating average time constants $\langle\tau\rangle$. We adopted a commonly used definition:[76,77]

$$\langle\tau\rangle = \frac{\int_0^{t'} \Delta A(t)\, dt}{\Delta A(0) - \Delta A(t')}$$

The average lifetime depends critically on the time constants of the slow components. Since the scans do not extend beyond 1 ns in our data, the time constants for components slower than 1 ns cannot be reliably determined. Therefore, we can only calculate the average lifetime within 1 ns. The results are shown in Table 2. The average ET rate (inverse of average time) clearly decreases as driving force increases. Although indicative of the relative rates, these average rates should only be used to qualitatively reflect the trend in these complexes.

The observed trend of decreasing back ET rate with increasing driving force is consistent with Marcus inverted region behavior. However, variations in electronic coupling in these catechol derivatives should also be considered. All catechol and the derivatives have the same anchoring group to $TiO_2$, and a similar $\pi$ electron-donating orbital. Except for 2,3-dihydroxynaphthalene, other derivatives differ by the nature of the substituent on the 3- or 4-position of the benzene ring. It is unclear how the substitution changes the electronic coupling strength. More importantly, unlike in the homogeneous solution, back ET from nanoparticles to adsorbates involves a distribution of trap states of different energy and distance. Despite these factors, a clear dependence on driving force is observed.

Evidence of Marcus inverted region back ET kinetics behavior was reported for $TiO_2$ nanoparticles sensitized by $Fe(II)(CN)_6^{4-}$ and derivatives[27] and $SnO_2$ particles sensitized by Ru polypyridyl dyes in the nanosecond time scale.[79] ET kinetics reported here is different from those in many dye-sensitized nanocrystalline thin films, which typically occur on the microsecond to millisecond time scale.[19−25] Theoretical studies[30,31,80] suggest that electron recombination kinetics depend on both the electron trapping/detrapping dynamics in the nanomaterials and the rate of ET at the trap sites.[30,80] As a result, the overall recombination kinetics depends on whether the trapping/detrapping rate or the ET rate is the rate-limiting step. If recombination is limited by the trapping/detrapping rate, its dependence on driving force may not be pronounced and rate is dictated by encountering rate of the electrons with the adsorbate sites.[19−24,31] On the other hand, if ET is the rate-limiting step, then Marcus inverted region behavior can be observed.[15,25,27,79,81,82] It may be reasonable to observe Marcus inverted region back ET kinetics in our case, since the fast back ET (<1 ns) is from electrons located near the adsorbate, for which diffusive encountering is probably not the rate-limiting step. On the >1 ns time scale, back ET probably involves electrons farther away from the adsorbate or at deeper trap sites. Whether their kinetics also show dependence on driving force remains to be examined.

## Summary

We have compared electron-transfer dynamics of a catechol−$TiO_2$ nanoparticle CT complex and an intramolecular CT complex, $[Ti(cat)_3]^{2-}$. ET rates are measured using ultrafast pump−probe spectroscopy. In both systems, 400 nm excitation of the CT bands promotes an electron from a catechol ligand to a Ti(IV) center(s). However, back ET kinetics in these systems are different. In the molecular complex, the back electron-transfer dynamics from the Ti(IV) center to catechol ligand occurs on the 200 fs time scale. In the adsorbate-to-nanoparticle complex, back ET is non-single-exponential with a 0.4 ps fast component and multiple slower components. The fast component is similar to that in the molecular complex and is attributed to electrons near the initial Ti center. The slower recombination components are attributed to the ability of electrons in nanoparticles to delocalize to other Ti(IV) sites farther away from the adsorbate.

Back ET from $TiO_2$ nanoparticles to catechol falls in the Marcus inverted region. We have also compared back ET kinetics to a series of catechol derivatives with varying redox potentials. We found that back ET kinetics in the subnanosecond time scale were highly non-single-exponential in all the complexes. The overall back ET process becomes slower as the relative driving force increases.

**Acknowledgment.** The work is supported by the National Science Foundation through Grants CHE-9733796 and CHE-0135427 and in part by the donors of the Petroleum Research Fund, and the Emory University Research committee. T.L. is an Alfred P. Sloan fellow. We thank Professor Joe Hupp for stimulating discussions and for sharing unpublished results on catechol/$TiO_2$ complexes.

## References and Notes

(1) Nazeeruddin, M. K.; Kay, A.; Rodicio, I.; Humphrybaker, R.; Muller, E.; Liska, P.; Vlachopoulos, N.; Gratzel, M. *J. Am. Chem. Soc.* **1993**, *115*, 6382.

(2) O'Regan, B.; Gratzel, M. *Nature* **1991**, *353*, 737.

(3) Serpone, N. *Res. Chem. Intermed.* **1994**, *20*, 953.

(4) Colvin, V. L.; Schlamp, M. C.; Alivisatos, A. P. *Nature* **1994**, *370*, 354.

(5) Asbury, J. B.; Hao, E.; Wang, Y.; Ghosh, H. N.; Lian, T. *J. Phys. Chem. B* **2001**, *105*, 4545.

(6) Asbury, J. B.; Ellingson, R. J.; Ghosh, H. N.; Ferrere, S.; Nozik, A. J.; Lian, T. *J. Phys. Chem. B* **1999**, *103*, 3110.

(7) Ellingson, R. J.; Asbury, J. B.; Ferrere, S.; Ghosh, H. N.; Sprague, J. R.; Lian, T.; Nozik, A. J. *J. Phys. Chem. B* **1998**, *102*, 6455.

(8) Heimer, T.; Heilweil, E. J. *J. Phys. Chem. B* **1997**, *101*, 10990.

(9) Tachibana, Y.; Moser, J. E.; Graetzel, M.; Klug, D. R.; Durrant, J. R. *J. Phys. Chem.* **1996**, *100*, 20056.
(10) Hannappel, T.; Burfeindt, B.; Storck, W.; Willig, F. *J. Phys. Chem. B* **1997**, *101*, 6799.
(11) Kalloinen, J.; Banko, G.; Sundstrom, V.; Korppi-Tommola, J. E. I.; Yartsev, A. P. *J. Phys. Chem. B* **2002**, *106*, 4396.
(12) Hao, E.; Anderson, N. A.; Asbury, J. B.; Lian, T. *J. Phys. Chem. B* **2002**, *106*, 10191.
(13) Ghosh, H. N.; Asbury, J. B.; Lian, T. *J. Phys. Chem. B* **1998**, *102*, 6482.
(14) Cherepy, N. J.; Smestad, G. P.; Gratzel, M.; Zhang, J. Z. *J. Phys. Chem.* **1997**, *101*, 9342.
(15) Martini, I.; Hodak, J. H.; Hartland, G. V. *J. Phys. Chem. B* **1998**, *102*, 607.
(16) Martini, I.; Hodak, J. H.; Hartland, G. V. *J. Phys. Chem. B* **1998**, *102*, 9508.
(17) Martini, I.; Hodak, J.; Hartland, G. V.; Kamat, P. V. *J. Chem. Phys.* **1997**, *107*, 8064.
(18) Moser, J. E.; Gratzel, M. *Chem. Phys.* **1993**, *176*, 493.
(19) Haque, S. A.; Tachibana, Y.; Klug, D. R.; Durrant, J. R. *J. Phys. Chem. B* **1998**, *102*, 1745.
(20) Tachibana, Y.; Haque, S. A.; Mercer, I. P.; Durrant, J. R.; Klug, D. R. *J. Phys. Chem. B* **2000**, *104*, 1198.
(21) Haque, S. A.; Tachibana, Y.; Willis, R. L.; Moser, J. E.; Graetzel, M.; Klug, D. R.; Durrant, J. R. *J. Phys. Chem. B* **2000**, *104*, 538.
(22) Hasselmann, G. M.; Meyer, G. J. *J. Phys. Chem. B* **1999**, *103*, 7671.
(23) Heimer, T. A.; Heilweil, E. J.; Bignozzi, C. A.; Meyer, G. J. *J. Phys. Chem. A* **2000**, *104*, 4256.
(24) Bach, U.; Tachibana, Y.; Moser, J.-E.; Haque, S. A.; Durrant, J. R.; Graetzel, M.; Klug, D. R. *J. Am. Chem. Soc.* **1999**, *121*, 7445.
(25) Kuciauskas, D.; Freund, M. S.; Gray, H. B.; Winkler, J. R.; Lewis, N. S. *J. Phys. Chem. B* **2001**, *105*, 392.
(26) Ghosh, H. N.; Asbury, J. B.; Weng, Y.; Lian, T. *J. Phys. Chem. B* **1998**, *102*, 10208.
(27) Lu, H.; Prieskorn, J. N.; Hupp, J. T. *J. Am. Chem. Soc.* **1993**, *115*, 4927.
(28) Vrachnou, E.; Vlachopoulos, N.; Graetzel, M. *J. Chem. Soc., Chem. Commun.* **1987**, 868.
(29) Liu, D.; Fessenden, R. W.; Hug, G. L.; Kamat, P. V. *J. Phys. Chem. B* **1997**, *101*, 2583.
(30) Nelson, J. *Phys. Rev. B: Condens. Matter Mater. Phys.* **1999**, *59*, 15374.
(31) Barzykin, A. V.; Tachiya, M. *J. Phys. Chem. B* **2002**, *106*, 4356.
(32) Weng, Y.-X.; Wang, Y.-Q.; Asbury, J. B.; Ghosh, H. N.; Lian, T. *J. Phys. Chem. B* **2000**, *104*, 93.
(33) Blackbourn, R. L.; Johnson, C. S.; Hupp, J. T. *J. Am. Chem. Soc.* **1991**, *113*, 1060.
(34) Vrachnou, E.; Vlachopoulos, N.; Gratzel, M. *J. Chem. Soc. Chem. Commun.* **1987**, 868.
(35) Doorn, S. K.; Stoutland, P. O.; Dyer, R. B.; Woodruff, W. H. *J. Am. Chem. Soc.* **1992**, *114*, 3133.
(36) Stoutland, P. O.; Dyer, R. B.; Woodruff, W. H. *Science* **1992**, *257*, 1913.
(37) Doorn, S. K.; Dyer, R. B.; Stoutland, P. O.; Woodruff, W. H. *J. Am. Chem. Soc.* **1993**, *115*, 6398.
(38) Reid, P. J.; Silva, C.; Barbara, P. F.; Karki, L.; Hupp, J. T. *J. Phys. Chem.* **1995**, *99*, 2609.
(39) Reid, P. J.; Barbara, P. F. *J. Phys. Chem.* **1995**, *99*, 3554.
(40) Walker, G. C.; Barbara, P. F.; Doorn, S. K.; Dong, Y. H.; Hupp, J. T. *J. Phys. Chem.* **1991**, *95*, 5712.
(41) Wang, C.; Mohney, B. K.; Akhremitchev, B. B.; Walker, G. C. *J. Phys. Chem. A* **2000**, *104*, 4314.
(42) Spears, K. G.; Wen, X. N.; Zhang, R. H. *J. Phys. Chem.* **1996**, *100*, 10206.
(43) Spears, K. G. *J. Phys. Chem.* **1995**, *99*, 2469.
(44) Spears, K. G.; Wen, X. N.; Arrivo, S. M. *J. Phys. Chem.* **1994**, *98*, 9693.
(45) Arnett, D. C.; Vohringer, P.; Scherer, N. F. *J. Am. Chem. Soc.* **1995**, *117*, 12262.
(46) Borgias, B. A.; Cooper, S. R.; Koh, Y. B.; Raymond, K. N. *Inorg. Chem.* **1984**, *23*, 1009.
(47) Bahnemann, D.; Henglein, A.; Lilie, J.; Spanhel, L. *J. Phys. Chem.* **1984**, *88*, 709.
(48) Moser, J.; Punchihewa, S.; Infelta, P. P.; Gratzel, M. *Langmuir* **1991**, *7*, 3012.
(49) Rodriguez, R.; Blesa, M. A.; Regazzoni, A. E. *J. Colloid Interface Sci.* **1996**, *177*, 122.
(50) Liu, Y.; Dadap, J. I.; Zimdars, D.; Eisenthal, K. B. *J. Phys. Chem. B* **1999**, *103*, 2480.
(51) Williams, G.; Watts, D. C. *Trans. Faraday Soc.* **1971**, *66*, 80.
(52) Pelizzetti, E.; Mentasti, E. *Z. Phys. Chem. (Wiesbaden)* **1977**, *105*, 21.
(53) Horner, L.; Geyer, E. *Chem. Ber.* **1965**, *98*, 2016.
(54) Land, E. J. *J. Chem. Soc., Faraday Trans.* **1993**, *89*, 803.
(55) Walhout, P. K.; Alfano, J. C.; Thakur, K. A. M.; Barbara, P. F. *J. Phys. Chem.* **1995**, *99*, 7568.
(56) Laubereau, A.; Kaiser, W. *J. Mod. Phys.* **1978**, *50*, 607.
(57) Owrutsky, J. C.; Raftery, D.; Hochstrasser, R. M. *Ann. Rev. Phys. Chem.* **1994**, *45*, 519.
(58) Bromberg, S. E.; Yang, H.; Asplund, M. C.; Lian, T.; McNamara, B. K.; Kotz, K. T.; Yeston, J. S.; Wilkens, M.; Frei, H.; Bergman, R. G.; Harris, C. B. *Science (Washington, DC)* **1997**, *278*, 260.
(59) Colombo, D. P.; Roussel, K. A.; Saeh, J.; Skinner, D. E.; Cavaleri, J. J.; Bowman, R. M. *Chem. Phys. Lett.* **1995**, *232*, 207.
(60) Colombo, D. P.; Bowman, R. M. *J. Phys. Chem.* **1995**, *99*, 11752.
(61) Colombo, D. P., Jr.; Bowman, R. M. *J. Phys. Chem.* **1996**, *100*, 18445.
(62) Rothehberger, G.; Moser, J.; Gratzel, M.; Serpone, N.; Sharma, D. K. *J. Am. Chem. Soc.* **1985**, *107*, 8054.
(63) Serpone, N.; Lawless, D.; Khairutdinov, R.; Pelizzetti, E. *J. Phys. Chem.* **1995**, *99*, 16655.
(64) Skinner, D. E.; Colombo, D. P.; Cavaleri, J. J.; Bowman, R. M. *J. Phys. Chem.* **1995**, *99*, 7853.
(65) Enright, B.; Redmond, G.; Fitzmaurice, D. *J. Phys. Chem.* **1994**, *98*, 6195.
(66) Rothenberger, G.; Fitzmaurice, D.; Gratzel, M. *J. Phys. Chem.* **1992**, *96*, 5983.
(67) Rajh, T.; Nedeljkovic, J. M.; Chen, L. X.; Poluektov, O.; Thurnauer, M. C. *J. Phys. Chem. B* **1999**, *103*, 3515.
(68) Rajh, T.; Poluektov, O.; Dubinski, A. A.; Wiederrecht, G.; Thurnauer, M. C.; Trinkunas, G. *Chem. Phys. Lett.* **2001**, *334*, 31.
(69) Persson, P.; Bergstroem, R.; Lunell, S. *J. Phys. Chem. B* **2000**, *104*, 10348.
(70) Stier, W.; Prezhdo, O. V. *J. Phys. Chem. B* **2002**, *106*, 8047.
(71) Marcus, R. A.; Sutin, N. *Biochim. Biophys. Acta* **1985**, *811*, 265.
(72) Steenken, S.; Neta, P. *J. Phys. Chem.* **1982**, *86*, 3661.
(73) Hagfeldt, A.; Gratzel, M. *Chem. Rev.* **1995**, *95*, 49.
(74) Henrich, V.; Cox, P. *The Surface Science of Metal Oxides*; Cambridge University Press: Cambridge, 1996.
(75) Lanzafame, J. M.; Palese, S.; Wang, D.; Miller, R. J. D.; Muenter, A. A. *J. Phys. Chem.* **1994**, *98*, 11020.
(76) Castner, E. W.; Maroncelli, M.; Fleming, G. R. *J. Chem. Phys.* **1987**, *86*, 1090.
(77) Maroncelli, M.; Fleming, G. R. *J. Chem. Phys.* **1987**, *86*, 6221.
(78) Martini, I.; Hodak, J. H.; Hartland, G. V. *J. Phys. Chem. B* **1999**, *103*, 9104.
(79) Dang, X.; Hupp, J. T. *J. Am. Chem. Soc.* **1999**, *121*, 8399.
(80) Nelson, J.; Haque, S. A.; Klug, D. R.; Durrant, J. R. *Phys. Rev. B: Condens. Matter Mater. Phys.* **2001**, *63*, 205321/1.
(81) Yan, S. G.; Prieskorn, J. S.; Kim, Y.; Hupp, J. T. *J. Phys. Chem. B* **2000**, *104*, 10871.
(82) Yan, S. G.; Hupp, J. T. *J. Phys. Chem.* **1996**, *100*, 6867.